Solar Energy Materials & Solar Cells 294 (2026) 113929

Contents lists available at ScienceDirect

Solar Energy Materials and Solar Cells

journal homepage: www.elsevier.com/locate/solmat

Experimental platform for PV generator characterization and MPPT algorithm simulation in vehicle integrated photovoltaic applications under real operating conditions

Edoardo Celi [a,*], Alessandro Minuto [a], Stefano Rizzi [a], Gianluca Timò [a], Alberto Dolara [b], Antonello Avella [b]

[a] RSE SpA, Via V. Callegari 21, 29122, Piacenza, Italy
[b] Politecnico di Milano, Via Lambruschini 4, 20156, Milano, Italy

ARTICLE INFO

Keywords:
Photovoltaic systems
Vehicles
VIPV
Partial shadings
DC-DC converter
MPPT

ABSTRACT

Vehicle Integrated Photovoltaic (VIPV) systems offer a promising solution to improve the sustainability of modern transportation. The motion of the vehicle leads to continuous changes in orientation of the photovoltaic (PV) generator, as well as dynamically varying partial shading. Maximizing energy harvesting in VIPV systems requires dedicated Maximum Power Point Tracking (MPPT) algorithms specifically designed to account for the dynamic variations of the PV generator's I-V curve under real conditions. This work presents the development of a comprehensive testing system for analysing the electrical behaviour of PV generators in VIPV applications and testing MPPT algorithms. A portable, high-speed I-V tracer was designed to acquire and store I-V curves of the onboard PV generator, along with irradiance and temperature measurements, every 0.5 s. The system has an autonomy of approximately 4 h, during which it can acquire up to 30000 I-V curves. The collected data is processed using two dedicated tools for statistical analysis and MPPT algorithm simulation and comparison. Preliminary measurement campaigns were carried out using a PV module mounted on the roof rack of an electric vehicle to validate both the hardware and software tools. A preliminary analysis shows that while the MPP voltage remains relatively stable, the MPP current shows rapid and significant changes due to dynamic irradiance. Three MPPT algorithms, Perturb & Observe, Constant Voltage, and a VIPV-specific method based on a patented technique, were simulated and compared. The VIPV-specific algorithm demonstrated a 2–8 % increase in harvested energy under dynamic conditions.

1. Introduction

Maximizing the energy production under highly dynamic vehicle operating conditions is one of the key challenges in vehicle integrated photovoltaics (VIPV) applications [1]. In these environments, photovoltaic (PV) modules are often subject to partial and dynamic shading caused by nearby buildings, trees or other vehicles. As a result, the maximum power point (MPP) of the module's power-voltage (P–V) curve can shift rapidly and unpredictably, requiring maximum power point tracking (MPPT) algorithms that are both fast and robust [2]. MPPT algorithms are implemented in the firmware of DC/DC converters, which are responsible for managing the energy transfer from the photovoltaic modules to the battery, electric motor, or auxiliary systems, while maintaining high conversion efficiency under all operating conditions.

Conventional MPPT techniques, such as *Perturb and Observe (P&O)*, are often inefficient in VIPV applications due to their slow convergence and limited accuracy, potentially working on local maxima rather than absolute ones [4,5]. While modern inverters for conventional PV systems attempt to mitigate this issue by scanning the full P-V curve every 5–10 min, such intervals are inadequate for the rapid environmental changes encountered by VIPV systems, as noted in several studies [4, 6–12].

Although significant research is aimed at developing high-

This article is part of a special issue entitled: PVinMotion2025 published in Solar Energy Materials and Solar Cells.

* Corresponding author.
E-mail addresses: edoardo.celi@rse-web.it (E. Celi), alessandro.minuto@rse-web.it (A. Minuto), stefano.rizzi@rse-web.it (S. Rizzi), gianluca.timo@rse-web.it (G. Timò), alberto.dolara@polimi.it (A. Dolara), anavella@unisa.it (A. Avella).

https://doi.org/10.1016/j.solmat.2025.113929
Received 4 June 2025; Received in revised form 14 August 2025; Accepted 27 August 2025
Available online 30 August 2025

performance MPPT algorithms, this effort for VIPV is severely hampered by a fundamental problem: the lack of experimental platforms designed for realistically testing and benchmarking them. The development and verification cycle of new MPPT strategies is basically constrained by the limitations of the tools available for their validation.

Various methods have been proposed in the literature to study MPPT behaviour under dynamic conditions, including hardware-in-the-loop systems, test setups with programmable irradiance, and software simulations based on synthetic or partially measured I-V curves. Although these approaches offer useful insights, they are often limited by idealized assumptions, limited real-world variability, or low sampling rates during data collection.

For example, San Josè et al. [3] proposed a method based on image processing to evaluate the performance of MPPT algorithms for VIPV systems during real urban driving. Their results showed that dynamic shading conditions significantly affect tracking efficiency, highlighting the need for context-specific MPPT strategies. Jankovec et al. [4] developed a mobile monitoring system to evaluate solar irradiance and PV module performance in dynamic environments. Their study demonstrated the difficulties in ensuring the accuracy of measurements on the move and highlighted the importance of synchronizing irradiance and electrical data for mobile PV applications.

A wide range of MPPT algorithms have been proposed in the literature, based on diverse operating principles such as perturbative, predictive, and evolutionary techniques. However, most of these algorithms have been developed for traditional, stationary photovoltaic systems and are not specifically optimized for the highly dynamic conditions typical of VIPV applications. Comprehensive reviews and/or test of these methods can be found in Refs. [13–16], which analyse MPPT performance under uniform and non-uniform irradiance conditions, as well as their adaptability to partial shading and load variations. As a matter of tact, MPPT algorithms for VIPV still remain to be developed, because most of them are limited to simulations or adapted from conventional PV inverters without VIPV-specific optimizations [17,18].

To address this critical testing gap, this paper introduces a novel experimental platform specifically designed for PV generator characterization and rigorous validation and benchmarking of MPPT algorithms in real VIPV scenarios. The core of our contribution is an integrated hardware and software setup whose components include: (i) a custom-designed, high-speed I-V tracer capable of acquiring full curves at approximately 0.5 s intervals; (ii) a custom “photovoltaic roof rack” on an electric vehicle with integrated, synchronized sensors; and (iii) a dedicated software environment enables post-processing of experimentally acquired data, as well as simulation, and fair comparison of different MPPT algorithms under identical conditions using real measured data.

To conduct real experiments for analysing VIPV system dynamics and identifying key performance indicators affecting the output, the customized “photovoltaic roof rack”, designed to preserve the vehicle’s aerodynamic profile and high safety standards, while enabling quick installation and removal, was mounted on a Renault Zoe electric vehicle. It includes a custom flexible silicon PV module designed for VIPV (installed in a flat aluminum plate), two irradiance sensors strategically positioned at the front and rear of the flat plane, and three temperature sensors mounted on the back of the PV module to monitor backsheet temperatures.

One of the key strengths of this approach is the ability to reproduce the entire sequence of measured I-V curves in the software environment, simulating the behaviour of various MPPT algorithms, including one specifically optimized for VIPV, under the same real conditions. This eliminates the variability typically encountered in field comparisons and allows for objective performance assessment.

Although the final objective is the development of a robust MPPT algorithm tailored for VIPV, starting from an MPPT algorithm originally developed and patented by RSE for conventional photovoltaic systems [19], this article primarily focuses on presenting the experimental platform that enables such development. Compared to existing state-of-the-art methods, this platform allows for faster sampling, more comprehensive data acquisition, and more accurate simulation of real operating conditions. We believe these features enable highly effective evaluation and comparison of MPPT strategies.

2. Experimental setup for analyzing VIPV system dynamics

To investigate the electrical behaviour of VIPV systems, under variable environmental condition, a proper experimental setup was developed.

The experimental setup consists of two main synergistic components: a customized hardware/firmware system for electrical and environmental data acquisition and a dedicated software platform for processing the high volume of measurements. The hardware system enables high-speed, high-resolution monitoring of the dynamic behaviour of key electrical parameters of the VIPV system under real conditions. The second is a dedicated software that first processes the resulting high-volume datasets to identify significant trends and anomalies and then provides a powerful simulation environment to compare the performance of various MPPT algorithms using filtered and processed real data.

The hardware part of the experimental setup consists of the following devices:

- A custom flexible silicon PV module, optimized for VIPV application (see Section 2.1).
- Two irradiance sensors, strategically positioned at the front and rear of the flat plane (see Section 2.2).
- Three temperature sensors, mounted on the back of the flexible silicon PV module to monitor backsheet temperatures (see Section 2.2).
- A custom-designed I-V tracer, capable of recording current-voltage (I-V) curves at a rate of approximately one measurement every 0.5 s. This acquisition speed significantly exceeds that of standard commercial devices, enabling accurate data capture even under rapidly fluctuating irradiance and non-uniformity of illumination conditions, commonly encountered in VIPV applications. The measurement electronics and data acquisition architecture, detailed in Section 2.3, are designed to operate reliably in highly unstable scenarios, supporting long-duration outdoor testing.

The first three devices listed were integrated into a custom-designed, non-invasive anchoring structure, referred to as the “photovoltaic roof rack”, to be installed on the roof of a Renault Zoe electric vehicle. It was engineered to preserve the vehicle’s aerodynamic profile and high safety standards, while enabling quick installation and removal. Its modular design allows for the integration of various types of photovoltaic modules and sensor configurations, making it suitable for testing under different environmental and operational conditions. During road tests, the I-V tracer prototype is housed inside the vehicle, with appropriate connections to the PV module and temperature and irradiance sensors mounted outside.

The data are then transferred from the I–V tracer’s memory to a PC equipped with the custom-developed software (see Section 3.1 and 4) for processing and analysis.

Fig. 1 shows the conceptual scheme of the experimental setup, including both hardware and software components, with a clear distinction between the data acquisition phase and the post-processing phase.

2.1. Custom flexible silicon module

During the design phase, careful consideration was given to optimizing the module layout, particularly in terms of geometric dimensions, number of cells (84 half-cut silicon cells - 130 mm × 65 mm), and the number of bypass diodes (N.6), in order to minimize power

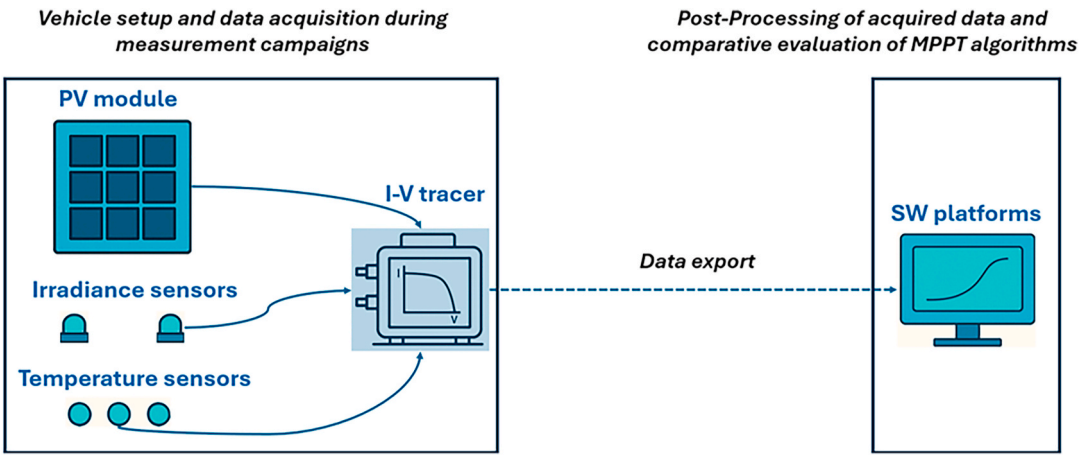

Fig. 1. Conceptual scheme of the experimental setup.

losses due to partial shading or non-uniform irradiance across the PV surface. A bypass diode is installed every 14 half-cells (equivalent to 7 full cells), whereas in most conventional PV modules, a diode is typically used to every 20 cells. The overall dimension of the module was defined based on the available surface area on the vehicle's roof, which amounts to approximately one square meter. Two VIPV modules, with the above reported specification, were developed by an Italian company, specialized in manufacturing flexible PV modules for vehicle integration. Table 1 and Fig. 2 respectively report and illustrate the characteristics of the PV modules. These modules are referred in the following to as *Module 1* and *Module 2*.

Module 1 was installed on the vehicle in a flat way, while *Module 2* was used for complementary testing.

The developed modules were subjected to a series of tests both in indoor and outdoor environments to verify their functionality and the consistency of the performance with the specifications. Indoor measurements were performed with the module under test connected to a Keithley 2430 electronic load using a four-wire configuration. To ensure the acquisition of the I-V curve in isothermal conditions, i.e. capturing each point of the I-V characteristic at the same temperature, a current ramp composed of 200 pulses was generated using the electronic load. The current was increased from zero to a maximum value Imax, corresponding to the expected short circuit current Isc under standard test conditions (STC). Each pulse had a duration of 5 ms, with a delay of 200 ms between successive pulses. The dark I-V curves were acquired with a measurement uncertainty of 0.5 % in both current and voltage. These curves were then interpolated using a method developed by RSE [20], which allows the evaluation of equivalent parameters of the PV module and its cells based on the following assumptions:

- The electrical behaviour of the module can be simulated using a single diode equivalent circuit model.
- All cells within the PV module show identical behaviour.

Table 1
Technical data of the silicon module for VIPV.

Maximum Power [W]	136.5
Thickness [mm]	2
Weight [kg]	1.9
Voltage of maximum power point: V_{MPP} [V]	47.9
Current of maximum power point: I_{MPP} [A]	2.85
Open circuit voltage: V_{oc} [V]	56.5
Short circuit current: I_{sc} [A]	3.0
PV strings x PV cells (n° cells)	6x14 (84)
N° of bypass diodes	**6**
Area [m^2]	0.8

The equivalent electrical parameters identified from indoor measurements are summarized in Table 2.

2.2. Sensors for measuring environmental data

The experimental setup includes a sensor system to monitor environmental factors that influence the performance of the *Module 1*. It features two GEOVES PIRSC pyranometers and three Texas Instruments DS18B20 temperature sensors, positioned to support effective data collection. The GEOVES PIRSC pyranometer measures global solar irradiance in the 400–1100 nm range. It uses a silicon photodiode with a 180° field of view and a cosine-corrected response. Each instrument is calibrated against a reference, with a typical daily uncertainty of less than ±3 % under clear sky. The sensor supports both voltage (0–5 V) and current (4–20 mA) outputs, ensuring measurements with short response time. To capture irradiance variations close to the PV module area, two pyranometers are used instead of one. While this solution does not provide full spatial mapping, it improves irradiance characterization compared to a single-point measurement and can be extended in future studies. Temperature data is collected using DS18B20 digital sensors, which offer the significant advantages of remarkably simple wiring via the 1-Wire protocol and intrinsic robustness to electrical interference, unlike analog sensors. These sensors measure temperatures from −55 °C to +125 °C with a typical accuracy of ±0.5 °C in the −10 °C to +85 °C range and offer programmable resolution between 9 and 12 bits. The three thermal sensors are positioned at two opposite corners and the centre of the module.

This combination of irradiance and temperature sensing supports the evaluation of PV module behaviour under operating, non-uniform conditions common in VIPV applications.

2.3. Prototype portable I-V tracer

A portable I-V tracer prototype was specifically designed to be compliant with the specific features of VIPV systems and the developed modules. Due to vehicle motion, both rapid fluctuations in solar irradiance and fast-changing partial shading could significantly modify the I-V curve in a very short time. To quantify the order of magnitude of the timescales over which the I-V curve can vary in VIPV applications, we can consider the following example. If we assume that the PV module described in section 2.1 moves at a constant speed of 50 km/h in the direction of its longest side (length of PV active surface 887 mm) and passes through a shaded area with its edge perpendicular to the direction of motion, the PV module operation would change from fully irradiated to fully shaded in 64 ms. However, considering the variation between individual solar cells within the module, this transition time for a single

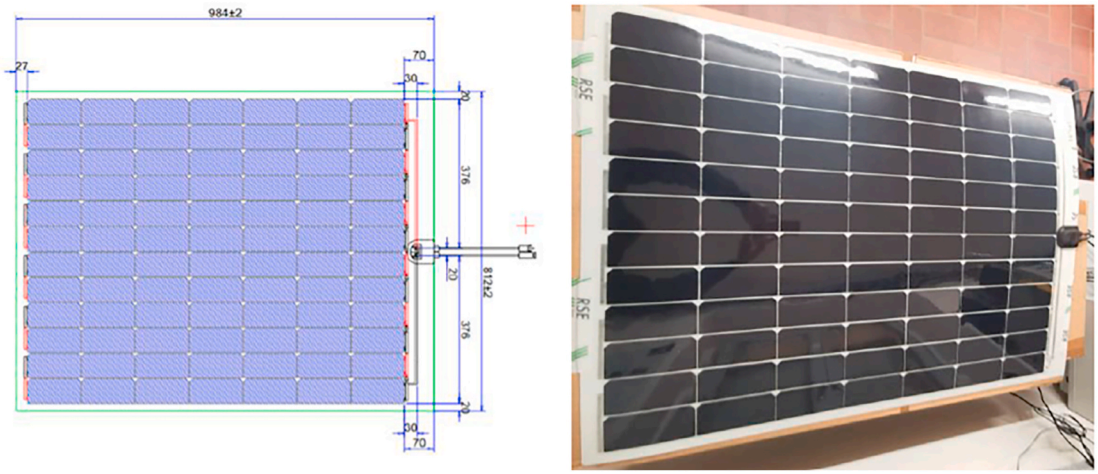

Fig. 2. Technical drawing and photo of the realized Module 1.

Table 2
Electrical parameters of the two silicon modules calculated by performing the dark I-V curve.

	Ideality Factor [a]	Series Resistance	Reverse Saturation Current [a]
	$N_{eq,cell}$	Rs mod [Ohm]	$I_{0eq,cell}$ [A]
Module 1	1.3965	0.4916	3.5119E-09
Module 2	1.4256	0.3409	4,7560E-09

[a] The values refer to a single PV cell. To calculate the ideality factor and the reverse saturation current of the module, this number must be multiplied by the number of cells in series (i.e. 84).

cell exposed to shading would be significantly shorter (a few milliseconds). On the other hand, the sweep for the measurement of the I-V curve requires voltage and current should be measured in quasi static conditions [21], i.e., the current due to the internal capacitance must be negligible compared to the output current. The I-V curve scan time increases with the required measurement accuracy and varies depending on the type of PV cells comprising the module: experimental results in Ref. [21] indicate 2.2 ms, 7.3 ms and 43.8 ms as the minimum scan times to keep the error below 0.5 % for 240 cm^2 polycrystalline, 240 cm^2 monocrystalline and 153 cm^2 back-contact silicon cells, respectively. It is worth noting that the duration of irradiance distribution transients related to VIPV applications may be comparable to or even faster than the minimum scan times of the I-V curve. For this reason, accurate measurement of the I-V curve during too fast irradiance distribution transients is not easily feasible. Achieving the hardware speed needed to capture these rapid changes is a considerable challenge, but we aimed to optimize our prototype to reduce scan time as much as possible, with a target acquisition time of 100 ms.

The technical specifications that guided the hardware design and software development of the portable I-V tracer were the following:

1. Reduced and adjustable I-V curve scan time, from minutes to a minimum of 100 ms.
2. Continuous scanning of the I-V curve, around two I-V curves per second.
3. Continuous measurement of irradiance and temperature sensors.
4. High computational and storage capacity (64 GB).
5. Simple and intuitive human-machine interface HMI.
6. Availability of standardized communication channels, such as I2C, SPI, etc., for connecting with discrete sensors, as well as digital input/output lines and standard USB and Ethernet ports.
7. Long battery operating time (more than 4 h).

The overall architecture of the portable I-V tracer is like that of the instrument presented in Ref. [22], however they differ in terms of measurement circuit, software, and sensors. Fig. 3 shows functional blocks of the portable I-V tracer.

The management and operation of the I-V tracer is overseen by a Raspberry Pi 4 Model B with 8 GB RAM (with a 7'' touchscreen display on the DSI port). The 1.8 GHz quad-core ARM Cortex-A72 CPU offers high computing power and supports parallel processing, while a 64 GB SD card ensures ample storage capacity. The touchscreen display provides a simple and intuitive interface for operating the I-V tracer, with an HMI layout resembling that of a smartphone app. Additionally, a wireless keyboard and mouse can be connected via Bluetooth, enabling remote operation in situations where direct access to the device is limited, such as for safety reasons.

The integrated circuit ADS1115 allows the Raspberry to read the differential analog outputs from irradiance sensors described in Section 2.2. ADS1115 is a precision, low-power, 16-bit, I^2C-compatible, ΣΔ analog-to-digital converter configurable for 4 single-ended or 2 differential inputs and operating at data rates of up to 860 samples per second.

A USB oscilloscope is used to acquire signals from the voltage and current sensors at the terminals of the PV module. This solution offers a ready-to-use, powerful, and flexible measurement platform. In particular, the Digilent Analog Discovery 2 provides two differential channels with 14-bit resolution and a 30 MHz bandwidth and is fully supported by libraries for developing custom applications and scripts in various programming languages. The measuring circuit is specifically designed to perform fast scans within a fixed scan time, while ensuring a complete acquisition of the I-V curve under all operating conditions of the photovoltaic generator, including variations in irradiance, partial shading, or other mismatch.

Among the available circuit topologies for I-V tracers [23], a unidirectional DC-DC converter was selected for this study. Capacitive load-based tracers tend to have slow scan times under low irradiance or partial shading, limiting their suitability for dynamic conditions. Bipolar power amplifiers, while precise, are inefficient and unsuitable for battery-powered systems. Four-quadrant H-bridge power supplies allow for both dark I-V and load-mode curve measurements but require an active DC bus with a voltage exceeding the PV system's open-circuit voltage. Electronic loads dissipate all power generated by the module, offering limited flexibility.

In contrast, DC-DC converters offer a more adaptable platform, supporting additional applications such as maximum power point tracking testing, which may require variable loads. For this research, a circuit based on a unidirectional Ćuk converter with a resistive load was developed. Adjusting the converter's duty cycle effectively changes the load, thereby controlling the voltage and current at the PV module

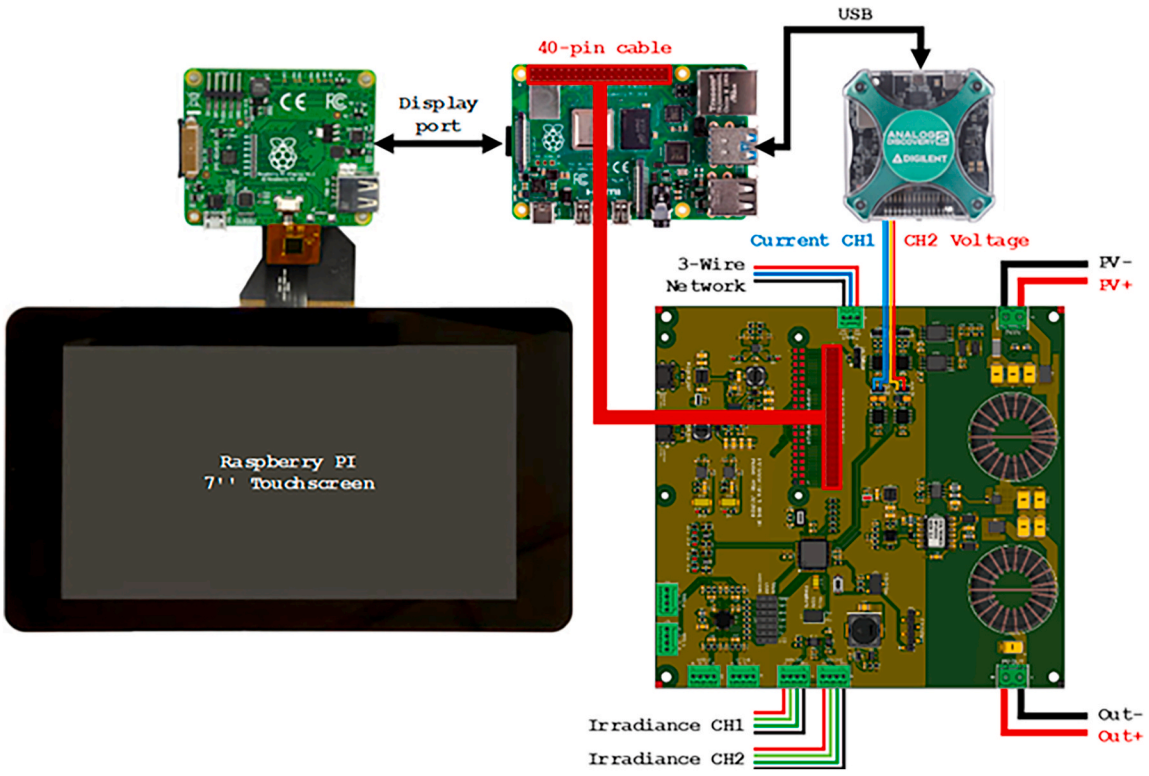

Fig. 3. Block diagram of the control and acquisition unit.

terminals. The Ćuk topology was chosen specifically for its low input current ripple, reducing the need for bulky filtering components and improving dynamic response. The entire system operates from a single 5V power supply. In this setup, a 20,000 mAh power bank was used, providing several hours of autonomous operation. The low-voltage requirement also makes the device compatible with USB car chargers, allowing continuous power during onboard testing. This 5V source powers the Raspberry Pi as well as all necessary conversion stages for the system's components.

A four layers Printed Circuit Board (PCB) was designed to implement all the hardware necessary for the operation of the I-V tracer, in particular (see Fig. 4):

- Ćuk converter, specifically designed and optimized for the PV module described in Section 2.1, including auxiliary circuits, controller and their power supplies.
- Two interfaces for irradiance sensors, which include both the 12V power supply for the sensor and the differential channel for irradiance measurement (0–5V signal).
- Interface for 1-Wire network.
- Voltage and current sensors, including analog signal conditioning circuits and their stabilized power supplies.
- Raspberry Pi interface with a 40-pin header; specifically, some pins are used for the 1-Wire network, the I^2C bus, and digital I/O for controlling the Ćuk converter.

To ensure safety and improved noise immunity, the Ćuk converter is electrically isolated from the control and measurement sections of the electronic board. Gate signals are supplied via an isolated driver, while isolated amplifiers are used to acquire voltage and current signals. All analog circuits and auxiliary components are powered via a flyback converter, ensuring complete galvanic isolation. The actual acquisition of voltage-current data occurs within 100 ms, while the remaining time (around 400 ms) is dedicated to auxiliary tasks such as data conversion and storage.

The acquisition of a single I-V curve exhibits linear computational complexity, denoted as O(N), where N represents the number of sampling points per curve. This is because the dominant operations, such as analog-to-digital conversion, data processing (e.g., filtering or normalization), and storage, are applied to vectors of length N. In the fixed-

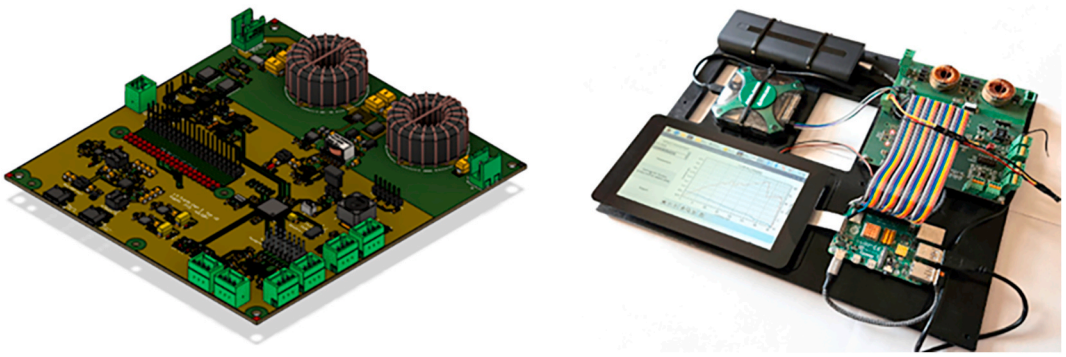

Fig. 4. On the left, the rendering of the I-V tracer board, while on the right, the I-V tracer prototype developed.

number acquisition mode, where a total of $N_{measures}$ I-V curves are sequentially collected, the overall computational complexity scales to O ($N_{measures}$ x N). Conversely, in continuous acquisition mode, where data is collected until an external stop condition is triggered, the total number of measurements is not defined a priori.

Therefore, the overall computational complexity cannot be precisely defined in advance and is inherently dependent on the actual duration and sampling rate of the session, although the per-measurement complexity remains O(N).

3. Measurement campaigns and preliminary results

The initial testing campaign focused on data collection under different operational conditions to evaluate the impact of environmental factors in both urban and non-urban contexts, was conducted in the Piacenza area (northern Italy). The main goal at this stage was not to establish cause-effect relationships, but to verify the proper functioning of the experimental setup (see Fig. 5), as well as ensuring the consistency of the acquired data. At this stage, the experimental hardware did not include additional tools, such as video cameras or GPS systems, that could directly correlate the solar irradiance distribution on the module surface with the corresponding I-V curve. The resulting datasets enabled a preliminary assessment of the system's performance under operating conditions and offered preliminary information on the PV system's response to partial shading and variable solar irradiance. The collected data, organized in folders containing I-V curves and environmental measurements, served as a validated basis for further analysis. The collected data required preliminary validation and filtering, which led to the development of the software described in the following subsection.

Fig. 5. "Photovoltaic roof rack" integrated on a company fleet vehicle during the measurement campaign.

3.1. Data processing software

The analysis software, developed in LabVIEW, processes data acquired by the custom I-V tracer to identify and exclude I-V curves that do not meet standard validity criteria. It also performs a detailed statistical analysis on the valid curves. The software accepts all XML files generated by the I-V tracer and outputs a cleaned dataset, from which non-conforming curves have been removed, along with the calculated statistical metrics (described in more detail below).

Curve validation is based on two main criteria: monotonicity and dimensionality. Non-monotonic I-V curves, typically caused by rapid irradiance fluctuations during acquisition, are flagged as invalid. Additionally, any curve containing fewer than N points (with N defined by the user) is considered incomplete or truncated and is discarded.

For statistical analysis, the software evaluates selected key parameters V_i , including the voltage and current of the maximum power point, the open-circuit voltage, the short-circuit current, the irradiance measured during each acquisition cycle, and the efficiency of the PV module.

The input data are divided into T subgroups (subsets) $V_{i,T} \in \{V_{i,1}, V_{i,2}, \ldots, V_{i,T}\}$ (with T defined as an input parameter), each consisting of elements $V_{i,t} = \{x_1, x_2, \ldots, x_Z\}$ *where* $Z = N/T$. For each subgroup and for each of the variables mentioned above, the following statistical metrics are computed: the mean μ, the variance σ^2, and the standard deviation σ. Thus, we obtain:

$$\mu_{i,t} = \frac{1}{Z}\sum_{j=1}^{Z} x_j \quad \sigma_{i,t}^2 = \frac{1}{Z}\sum_{j=1}^{Z}\left(x_j - \mu_{i,t}\right)^2 \quad \sigma_{i,t} = \sqrt{\sigma_{i,t}^2} \qquad 1$$

Furthermore, it is possible to conduct more targeted analyses by calculating the same statistical quantities on the elements included between the indices/number of samples "I" and "F" (also defined as input parameters), thus allowing the examination of a specific dynamics after having identified the initial and final moments of interest. All these metrics are presented both in tabular form and through graphs, specifically chosen to facilitate the understanding of the results. The following statistical metrics is then used:

$$\mu_{i,I\ldots F} = \frac{1}{F-I+1}\sum_{j=I}^{F} x_j \quad \sigma_{i,I\ldots F}^2 = \frac{1}{F-I+1}\sum_{j=I}^{F}\left(x_j - \mu_{i,I\ldots F}\right)^2 \quad \sigma_{i,I\ldots F} = \sqrt{\sigma_{i,I\ldots F}^2} \qquad 2$$

Error bar graphs were chosen for each variable to simultaneously display mean and standard deviation. In addition, separate graphs of standard deviation and its evolution over time were created, providing a detailed view of the behavior of the analysed electrical variable during the entire acquisition process.

3.2. Preliminary results of the dynamics study

This chapter details the results of a comprehensive measurement campaign. These tests were performed on mixed road routes under mostly clear sky conditions, with intermittent cloudiness during a summer day in 2024, when the high solar altitude minimized the impact of partial shading.

A total of 9288 I-V curves were acquired (dataset called *Test 1*). Temperature measurements were taken every 100 samples, i.e. every 100 acquisitions of I-V curves and irradiance values measured by solarimeters. After applying the pre-filtering and filtering steps, the number of valid I-V curves available for further analysis was reduced to 8012, resulting in a discard rate of about 14 %. This reduction is mainly due to the elimination of I-V curves that did not meet the established criteria, such as those affected by incorrect readings or inadequate operating conditions.

The average irradiance values (Global Tilted Irradiance, GTI) on the plane of the "photovoltaic roof rack", measured by the two solarimeters,

are shown in Fig. 6. A high variability can be observed, except in the central part of the test (sample interval between 4000 and 4500), where the irradiance exhibited a gradual and slow transition, increasing from very low values around 200 W/m^2 to approximately 700 W/m^2. This condition occurred with the vehicle stationary and the gradual increase in irradiance is due to the clearing of the cloud cover. Figs. 7 and 8 show the values of voltage (Voc and V_{MPP}) and current (Isc and I_{MPP}) respectively. It can be noted that the voltage of the maximum power point V_{MPP} shows low intensity variations, while the current values I_{MPP} show larger and more frequent fluctuations. This behavior aligns with variations in solar irradiance, given the direct proportionality between current and irradiance incident on the PV cells, while voltage changes logarithmically. The statistical analysis of the four electrical quantities and solar irradiance was performed using a subset size of 1000 samples. As detailed in the previous section, the statistical analysis involved representing the means and standard deviations (with k = 1) for each subset using error bar charts, allowing for a clear visual interpretation of parameter variation and dispersion.

Fig. 9 displays the mean values and standard deviations of V_{MPP} across the time slots. The data analysis shows that, apart from subset 1 and 4, where the standard deviations reached notable values (6 V and 4.5 V, respectively), the variability remained limited throughout the rest of the test, with standard deviations below 2 V. The average V_{MPP} values were relatively stable, fluctuating between 47 V and 48 V, consistent with the voltage trends shown in Fig. 7 and the nominal value reported in Table 1. The statistical graphs for I_{MPP}, shown in Fig. 10, indicate that the average current of the maximum power point remained around 1.5 A, with standard deviations that, while remaining stable, were around 0.5 A. These standard deviation values are relatively high compared to the mean, highlighting once again the impact of the disturbed and dynamic conditions typical of VIPV applications, particularly on the maximum power point current.

The statistical analysis of solar irradiance, presented in Fig. 11, further supports these findings. Fluctuations in irradiance, caused by changing environmental conditions and dynamic partial shading, play a critical role in determining the variations in the observed electrical quantities, directly influencing the stability and performance of VIPV systems.

As mentioned, the temperature values measured by the three sensors were stored every 100 samples (approximately every minute). This sampling frequency was chosen to limit the volume of data and accommodate the extended measurement period, based on the assumption that temperature would not change drastically within seconds. The analysis of the data, shown in Fig. 12, indicates that the selected sampling period of the thermal sensors is sufficient to represent the general trend of temperatures.

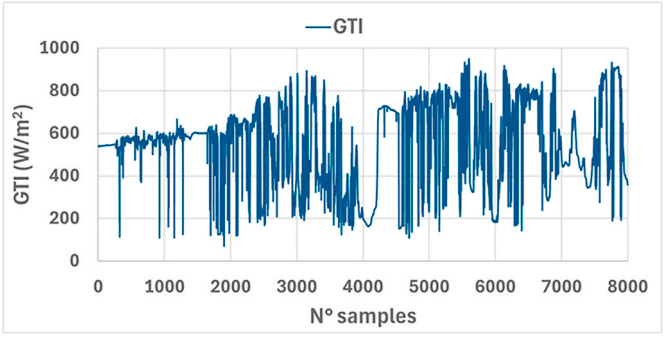

Fig. 6. Global tilt irradiance profile recorded during the measurement session. The irradiance data shows frequent and rapid fluctuations, mainly due to urban driving conditions and dynamic shading effects caused by buildings, trees, etc. This highly dynamic irradiance profile is representative of realistic VIPV scenarios.

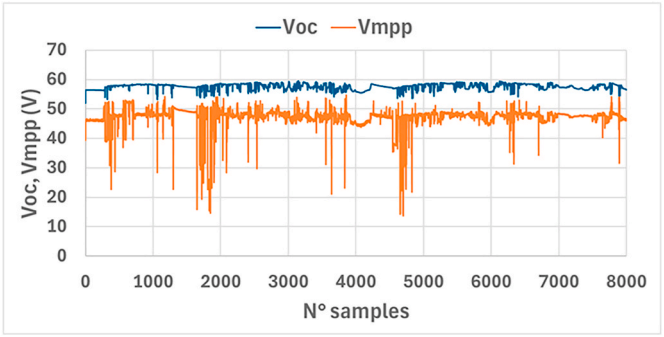

Fig. 7. Behaviours of the open circuit voltage Voc, and of the maximum power point voltage V_{MPP}, extracted from I-V curve measurements during the measurement campaign. While Voc remains relatively stable despite irradiance fluctuations, V_{MPP} exhibits significant variations, particularly during irradiance dips, highlighting the need for MPPT algorithms that can accurately and rapidly track dynamic variations.

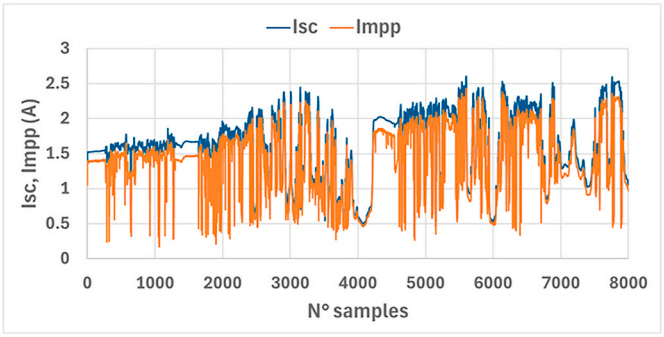

Fig. 8. Behaviours of the short circuit current Isc, and of the maximum power point current I_{MPP}, obtained by processing the I-V curves acquired during the measurement campaign. The strong correlation between Isc and I_{MPP} is broken during periods of partial shadings or irradiance transients, when I_{MPP} shows rapid drops.

3.3. Example of I-V and P-V curves acquired during the campaigns

Some of the I-V and P-V curves acquired during the experimental sessions were particularly significant (see Fig. 13), especially with regard to their rapid dynamics observed in extremely short time intervals. The curves obtained in dynamic conditions show points of absolute maximum power located in voltage coordinates that differ significantly from the nominal values.

The *Module 1*, based on half-cut cells, exhibited I-V curves that differed significantly from those measured on standard full-cell silicon modules under mismatch conditions. Notably, under partial shading or rapidly changing irradiance, the module showed signs of reverse bias behaviour and multiple power peaks in the P-V curve, along with corresponding current steps in the I-V curve, often exceeding the number of bypass diodes. This behaviour has been attributed to the relatively low reverse breakdown voltage of half-cut cells, which makes them more prone to localized reverse bias. As a result, the I-V curve may have nonlinearities, and inflection points that complicate maximum power point tracking and raise potential concerns about long-term reliability if such conditions occur frequently.

These I-V dynamic behaviours, especially localized reverse bias and multiple power peaks, are closely associated with known reliability issues, particularly in long-duration static conditions (e.g., on rooftops), such as the formation of hot spots. According to Özkalay et al. [24], partial shading can cause hot spots even at moderate temperatures, including in advanced cell types such as PERC, IBC, and HJT. In their tests, IBC modules, like those used in this study, exhibited greater

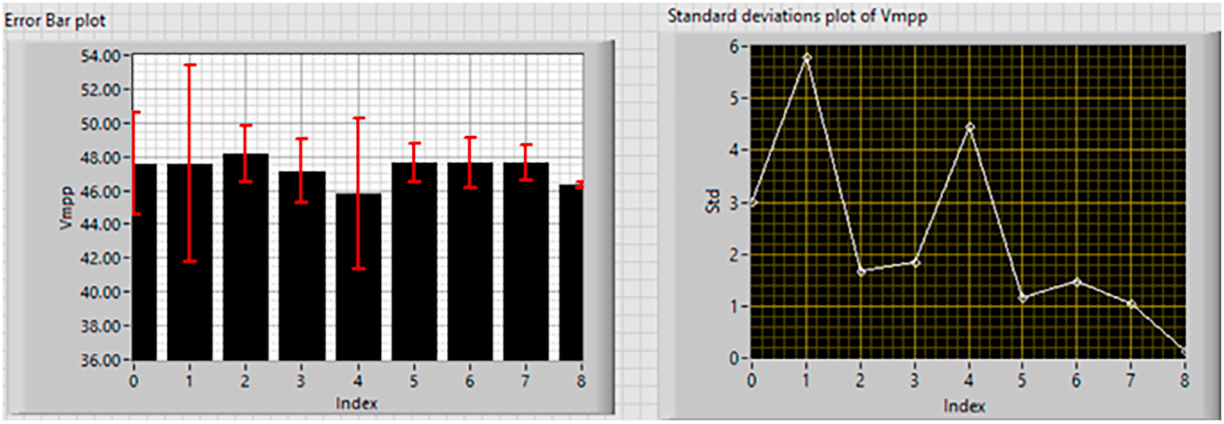

Fig. 9. Quantitative analysis of V_{MPP} instability during the road test. The error bar graph on the left shows the average V_{MPP} for different time slots, with the size of the error bars indicating the degree of voltage fluctuation. The graph on the right explicitly quantifies this variability by plotting the standard deviation, highlighting time slots with high dynamics (e.g., indices 1 and 4) compared to more stable periods (e.g., index 8).

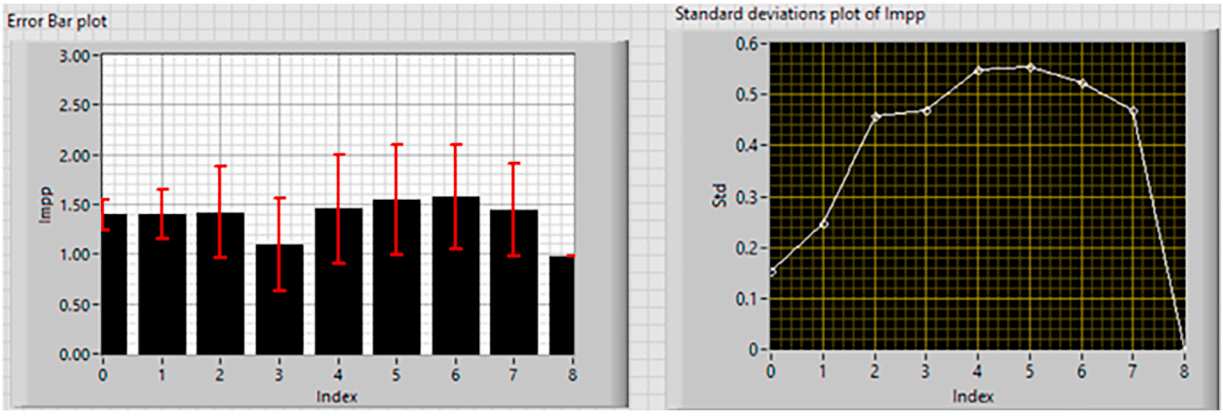

Fig. 10. Statistical analysis of the I_{MPP}. The graph on the left shows the average current per time slot, while the graph on the right quantifies the trend of the maximum power point current via its standard deviation. It is observed that the real test conditions were more dynamic during sessions 4, 5, and 6.

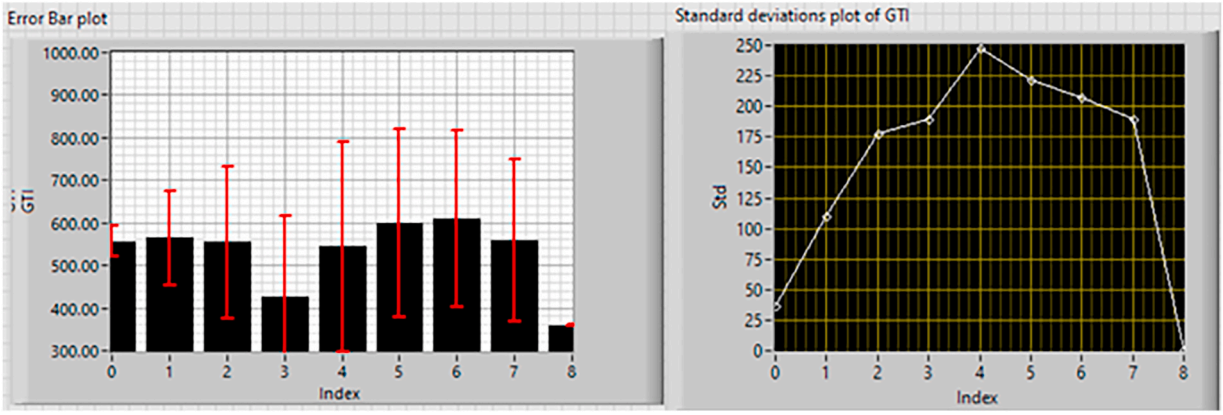

Fig. 11. On the left, the error bar of the solar irradiance incident on the "PV roof rack", while on the right, the behaviour of its standard deviation. As shown in Fig. 6, solar irradiance varied significantly throughout the test, except in the initial and final segments, where lower variability corresponds to prolonged vehicle stops during these periods.

resilience thanks to diode functionality, uniform heating, and lower breakdown voltage. In VIPV systems, partial shading is generally transient, which, combined with airflow cooling, reduces cumulative thermal stress and hot-spot risk, although prolonged stationary periods (e.g., parked vehicles) can still present hazards.

Cloud edge effects [25] can also occur, where cloud edges concentrate sunlight into brief irradiance spikes, challenging the MPPT response and causing short-term mismatch or thermal stress. Our high-speed IV tracking may enable future studies of hotspots and cloud edge effects under real VIPV conditions.

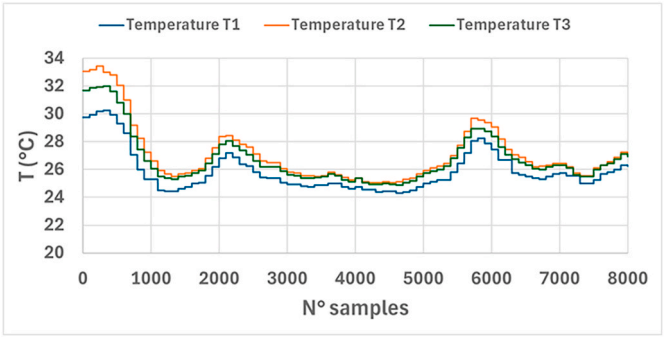

Fig. 12. Backsheet temperature of the Module 1 recorded during the measurement campaign at three different points (T1, T2, T3). The graph shows that the temperature evolves slowly and uniformly across the module, in stark contrast to the rapid, high-frequency fluctuations observed in the irradiance and electrical data.

4. Software for testing MPPT algorithms with experimentally acquired I-V curves and results

The experimentally acquired I-V curves can be used to test different MPPT algorithms under the same conditions, including the VIPV-specific MPPT algorithm, developed by the authors and described briefly in the chapter 4.2. This allows for an evaluation of the strengths and weaknesses of each MPPT algorithm based on the environmental and boundary conditions that affect the VIPV system.

To carry out these comparative tests, a software tool was developed in Labview environment, mainly consisting of two distinct programs: an I-V curve emulator and an MPPT algorithm simulator. The need to develop an I-V curve emulator arises from a fundamental limitation of the experimental setup: the prototype I-V tracer, although fast, can only sample an I-V curve approximately every 500–600 ms. Due to this limitation, which has led to the filtering of unphysical I-V curves, the dynamics and transient phenomena that occur between samples remain largely uncaptured. This is a significant problem, since variations can occur even within a few milliseconds when the vehicle is in motion (as explained in Section 3.2). On the other hand, real control systems, such as inverters or DC/DC converters connected to a PV system, operate according to the MPPT algorithms implemented in the control firmware, executing decisions in much shorter time intervals, typically on the order of milliseconds or tens of milliseconds. Therefore, it was important to develop a method capable of realistically reconstructing and defining the transient states that occurred between one experimentally acquired I-V curve and the next.

4.1. SW MPPT tester

MPPT Tester is the main LabVIEW-based program developed to evaluate MPPT algorithms using experimentally acquired I-V curves. The simulation operates synchronously: the I-V curve emulator advances through the I-V curves only after the MPPT algorithm completes each processing step. (see Fig. 14).

The system consists of four main blocks: *Parameters*, *MPPT Algorithm*, *Outputs*, and the *VIPV Module Emulator*. These blocks operate in parallel and exchange information during execution through synchronization mechanisms such as Queues FIFOs, Shared Variables, and Semaphores. Fig. 15 displays the software's graphical user interface, enabling user interaction and summarizing the block diagram section within the LabVIEW environment.

4.1.1. Parameters

Parameters block represents a component primarily oriented toward the frontend. Its main function is to acquire all the necessary information from the *Parameters* section of the graphical user interface. This information is essential for feeding both the *MPPT Algorithm* and the *Outputs* sections, enabling them to conduct their respective processes. The collected parameters are transmitted to the *MPPT Algorithm* and *Outputs* blocks only once, at program startup, thus ensuring that both blocks have all the initial settings required for proper operation.

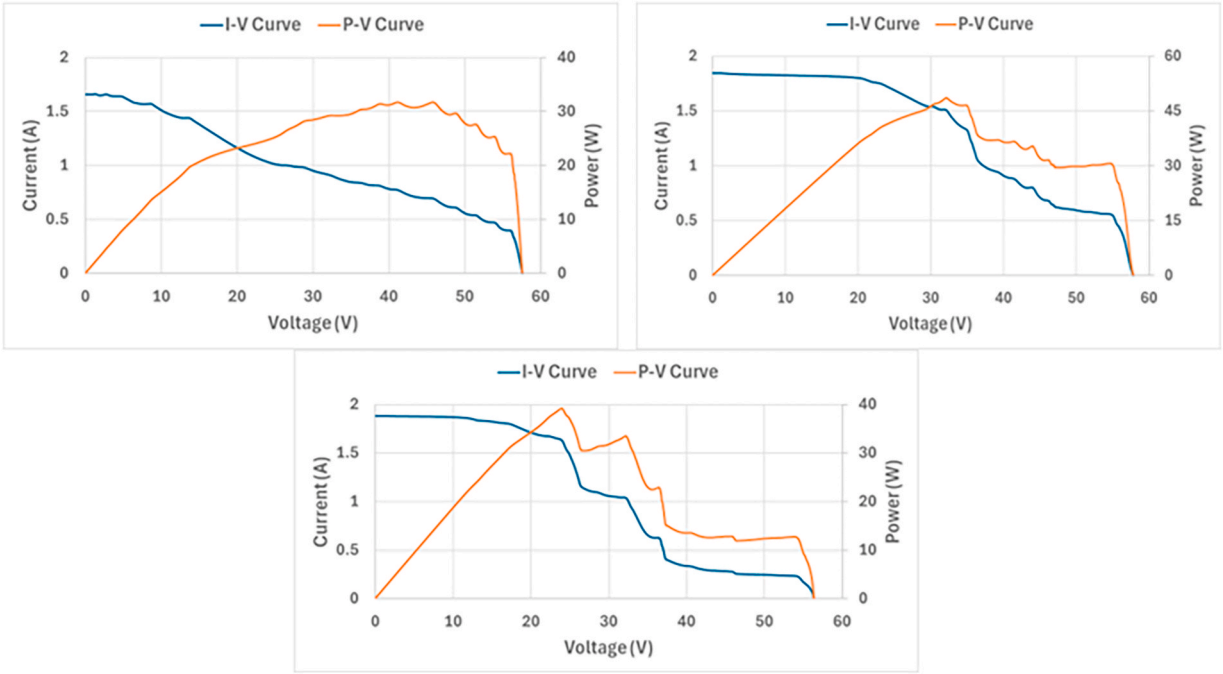

Fig. 13. Examples of different and complex I-V curves (in blue) and P-V curves (in orange), generated by the half-cut cell module under real partial shading conditions. A key characteristic of this technology is the appearance of multiple power peaks, often exceeding the number of bypass diodes. The figure presents three distinct measured I-V (P–V), demonstrating how the global maximum power point can be located at very different voltages (e.g., 45 V, 32 V, and 25 V), requiring a highly adaptive MPPT strategy.

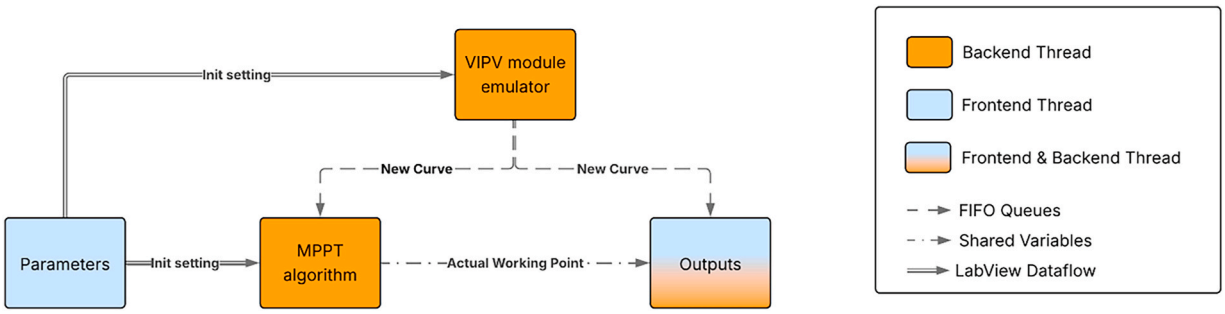

Fig. 14. Block diagram of the MPPT tester SW.

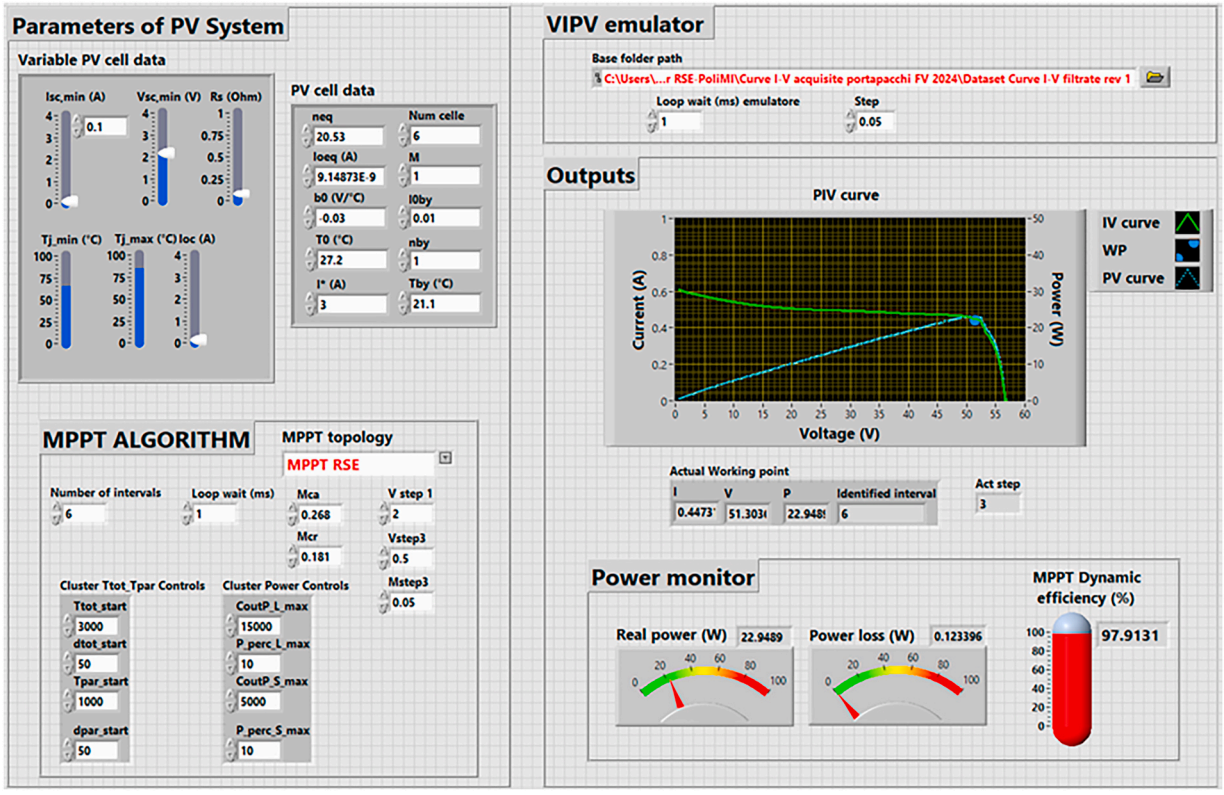

Fig. 15. Graphical user interface (LabVIEW environment) of the MPPT tester SW.

4.1.2. MPPT algorithm

MPPT Algorithm is a backend-focused block that implements the MPPT algorithm under test. During execution, this block continuously updates the actual operating point of the system V_{act} in the case of voltage control or I_{act} in the case of current control, to track the maximum power point in real time. The MPP shifts in response to changes in environmental conditions affecting the PV system. To communicate the updated operating point to the *Outputs* block and to other internal modules within the *MPPT Algorithm* block itself, shared variables are used. To prevent potential inconsistencies caused by simultaneous read/write operations on these shared variables, the use of semaphores has been integrated. This approach allows for the offline evaluation and comparison of different tracking strategies under dynamically varying irradiance and shading conditions, closely replicating real VIPV behaviour without requiring real-time hardware interaction.

4.1.3. Outputs

The *Outputs* block integrates both backend and frontend components to monitor and display the status of the *MPPT algorithm* and the *VIPV Module Emulator*. On the backend, it calculates the theoretical maximum power point (V_{MPP}, I_{MPP}), while the frontend manages the real-time visualization of the current I-V curve, the MPPT algorithm's operating point, and key performance indicators. These include actual power, power loss, and, most importantly, the *dynamic MPPT efficiency*, which provides immediate visual feedback on the algorithm's performance. As defined by the IEC 62891 ED1 (*Overall efficiency of grid connected photovoltaic inverters*), the *MPPT efficiency* is the ratio of the energy drawn by the device under test within a defined measuring period T_M to the energy provided theoretically by the PV emulator in the maximum power point (eq. (3)). This quantity has been used as the primary benchmark for comparing MPPT algorithms under identical test conditions.

$$EFF_{MPPT,dyn} = \frac{1}{\sum_j P_{MPP,PVs,j} \times \Delta T_j} \times \sum_i V_{DC,i} \times I_{DC,i} \times \Delta T_i \quad (3)$$

With:

- $P_{MPP,PVs,j}$ is the maximum power provided by the PV simulator.

- $V_{DC,i}$ is the sampled value of the inverter's input voltage.
- $I_{DC,i}$ is the sampled value of the inverter's input current.
- ΔT_j is the period in which the power $P_{MPP,PVs,j}$ is provided.
- ΔT_i is the period in which the power $V_{DC,i}$ and $I_{DC,i}$ are sampled.

To ensure real-time updates, the *Outputs* block accesses shared resources such as shared variables and queued FIFOs, with semaphores used to manage synchronization and maintain data integrity during concurrent read/write operations.

4.1.4. VIPV module emulator

The *VIPV module emulator* block simulates the behavior of a VIPV system by leveraging the I-V curves acquired by the I-V tracer. At each iteration, it reads two consecutive I-V curves, {V_1, I_1} and {V_2, I_2}, each consisting of N data points, and performs linear interpolation between them. In doing so, it estimates the evolution of intermediate curves $\left\{V_i^{(k)}, I_i^{(k)}\right\}$ *with* $k = 0,1,2,\ldots,K$, which were not directly acquired, effectively increasing the apparent sampling frequency compared to the actual hardware rate. In this case, the interpolation step $\Delta\alpha \in (0,1]$ is provided as an input parameter and determines the number of intermediate curves to estimate, $K = \left\lfloor \frac{1}{\Delta\alpha} \right\rfloor$. Thus, each point of the intermediate curves is estimated as follows:

$$V_i^{(k)} = (1-\alpha_k)V_{1i} + \alpha_k V_{2i} \quad (4)$$

$$I_i^{(k)} = (1-\alpha_k)I_{1i} + \alpha_k I_{2i} \quad (5)$$

With $i \in [1,N]$ $\quad \alpha_k = k\Delta\alpha$

To support continuous simulation during execution, the emulator uses a pair of FIFO queues (each with a 15-element capacity), implementing a producer-consumer architecture. The *VIPV module emulator* acts as the producer, generating interpolated curves, while the *MPPT algorithm* acts as the consumer. The queues handle the transfer of curves between different components of the *MPPT Tester*, ensuring thread-safe communication. As for the other blocks, to avoid data inconsistencies due to concurrent access, semaphores are employed for synchronized read/write operations.

4.2. VIPV-specific MPPT algorithm

The *VIPV-specific MPPT algorithm* represents an optimized version of an MPPT algorithm developed and patented by RSE in recent years for traditional and concentrated PV systems [19,26]. It is based on a mathematical approach that enables the rapid comparison of local maxima on the P-V curve to identify the global maximum power point without requiring a full scan of the I-V curve. This method efficiently finds the voltage interval, called the *target voltage range*, where the global peak is located, and then operates an optimized *Perturb and Observe* routine within that interval. A key concept to understand such MPPT algorithm is the *canonical interval*. For a PV module/system composed of N substrings affected by partial shading (electrical mismatch), the *k*-order *canonical interval* (called I_k) is the voltage range where *k* substrings are active (producing voltage), while the remaining *N-k* are bypassed via their respective bypass diodes. The full I-V curve is defined within the voltage range (0-Voc), which is the union of all *canonical intervals*. The *target voltage range* always corresponds to one of these *canonical intervals*.

The goal of this algorithm is to quickly identify this *target voltage range*. To do so, it requires prior knowledge of the PV system configuration, such as the number of modules connected in series/parallel and the number of bypass diodes. The algorithm operates in four main steps: the first three identify the *target voltage range*, while the final step applies an optimized *P&O* routine to accurately track the maximum power point.

In the current studies on VIPV applications, the described software, along with previously developed tools, has enabled code optimization aimed at improving the algorithm performance under the highly dynamic and challenging conditions typical of VIPV systems. Specifically, key algorithm parameters have been refined, and automatic retriggering conditions have been adjusted to ensure continuous and accurate MPP tracking during rapid changes of the I-V curve.

4.3. First dynamic tests and performance comparisons between MPPT algorithms

Following the development of the *MPPT Tester* software, initial tests were conducted to compare the energy performance of different MPPT algorithms, including the one developed and optimized for VIPV application by the authors. The MPPT algorithms currently implemented in the software include *Perturb & Observe* and *Constant Voltage*, as they are among the most widely used and easiest to implement in an initial version of the software, in addition of course to the *VIPV-specific MPPT algorithm*. The platform is designed for flexibility and can be extended to support any MPPT algorithm, provided that its operating states are known.

It is important to note that the current simulation environment does not include interaction with hypothetical power conversion hardware or physical loads. Consequently, the *dynamic MPPT efficiency* assessment does not consider the transients introduced by the generation and conversion systems, which could be addressed in future developments.

Table 3 presents the results of the initial dynamic comparison tests, based on the *dynamic MPPT efficiency* values achieved by the different algorithms. These results reflect the algorithm performance in response to the time-varying electrical conditions sampled during the measurement campaign described in chapter 3 (called *Test 1*), as well as in additional validation tests.

The dataset referred to as *Test 2* was collected during a measurement campaign conducted in the summer period, along mixed driving routes (urban and extra-urban areas). It includes a slightly larger volume of electrical and environmental data compared to the dataset discussed so far within the article. As shown in Table 3, the results are highly consistent with previous findings and further confirm that the *VIPV-specific MPPT algorithm* can process a greater amount of energy by reducing power losses under disturbed conditions, compared to the conventional MPPT algorithms tested. *Test 3*, on the other hand, corresponds to a much shorter measurement campaign (approximately 10 min), entirely characterized by highly disturbed and dynamic operating conditions. The *dynamic MPPT efficiency* values obtained in this scenario highlight how, under certain challenging conditions, the performance gap between a robust, adaptive MPPT algorithm and simpler, conventional approaches can significantly widen.

These results reinforce the conclusion that MPPT performance is highly dependent on the specific case study and boundary conditions.

Although a detailed analysis of computational complexity, convergence speed, and robustness was not the main objective of this work, the reported results, particularly those from Test 3, provide indirect evidence of the proposed algorithm's faster adaptation and improved

Table 3
Dynamic MPPT efficiency comparison between the VIPV-specific algorithm, Perturb & Observe, and Constant Voltage methods across three datasets. The VIPV-specific algorithm consistently achieves higher performance, particularly under highly dynamic conditions (Test 3, a short 10 min session), demonstrating greater adaptability and energy extraction capability.

	Dataset	N° of I-V curves	*VIPV-specific MPPT algorithm*	*Perturb & Observe*	*Constant Voltage*
Dynamic MPPT efficiency	Test 1	8012	99.4 %	97.7 %	96.8 %
	Test 2	10773	99.7 %	98.2 %	97.0 %
	Test 3	986	91.7 %	83.9 %	83.9 %

tracking behaviour. The flexibility of the experimental platform allows for future extensions that could include both static and dynamic evaluations of these metrics across multiple algorithms under diverse and realistic conditions.

5. Conclusions

This work presented the development and validation of a comprehensive experimental testing platform specifically developed for VIPV applications, enabling detailed analysis of the electrical behaviour of PV generators and systematic evaluations of MPPT algorithms.

Fast and continuous I-V curve measurements are essential for understanding and analysing the operation of a VIPV generator under rapidly changing irradiance and shading conditions caused by vehicle motion. To meet these specific requirements, a custom-designed, portable I-V tracer was developed. The tracer can acquire a full I-V curve with a scan time of 100 ms, while the complete measurement cycle, including irradiance and temperature acquisition and data logging, has a total duration of approximately 500 ms, outperforming commercial devices in terms of sampling rate and data logging.

Specific software tools were developed for data validation, data analysis and MPPT algorithm simulations. The trends of key electrical parameters, such as open-circuit voltage, short-circuit current, maximum power, and the related voltages and currents, are analysed by the statistical tool to examine and summarize their variability during a test campaign. The I-V curve sequences were used as input dataset for the MPPT algorithm simulation tool, which supports the implementation of any MPPT algorithm, evaluates the power output of the implemented control logic under real operating conditions, and enables the comparison of different control strategies in terms of dynamic MPPT efficiency.

Three experimental campaigns were conducted on mixed urban and extra-urban driving scenarios; in a single measurement campaign over 9000 I-V curves were recorded in real operating conditions and approximately 8000 were considered valid. Preliminary statistical analysis confirmed that the MPP voltage generally remains close to the value observed under uniform irradiation and does not exhibit large fluctuations. However, unlike photovoltaic systems, its variations are more frequent and pronounced due to the dynamic operating conditions of VIPV. In comparison, the MPP current shows more significant and rapid changes, strongly correlated with fluctuations in solar irradiance. These results suggest that, for the PV generator analysed, operating conditions involving partial shading are relatively limited in duration but still induce noticeable variability in electrical behaviour.

Temperature trends were consistent with expected thermal inertia and did not significantly impact short-term dynamics.

The dataset served as input to simulate realistic operating conditions in the MPPT test environment. Three MPPT techniques were considered: *Perturb & Observe*, *Constant Voltage*, and a *VIPV-specific MPPT algorithm* based on a patented MPPT technique designed to address the mismatch effects caused by partial shading. The results showed that the VIPV-specific MPPT algorithm outperformed conventional strategies in all tested scenarios, achieving up to 99.7 % dynamic tracking efficiency and increasing harvested energy by 2 %–8 %, especially under rapidly changing irradiance and partial shading conditions.

Future work will focus on increasing the scanning speed of the I–V tracer to obtain more valid data and achieve higher temporal resolution. Additionally, efforts will be directed at building a significantly larger experimental database to provide statistically relevant results, as well as expanding the set of MPPT algorithms used for comparison.

CRediT authorship contribution statement

Edoardo Celi: Writing – review & editing, Writing – original draft, Validation, Supervision, Software, Data curation, Conceptualization. **Alessandro Minuto:** Validation, Supervision, Methodology. **Stefano Rizzi:** Conceptualization. **Gianluca Timò:** Writing – review & editing, Supervision. **Alberto Dolara:** Writing – review & editing, Software, Data curation, Conceptualization. **Antonello Avella:** Software, Data curation.

Declaration of generative AI and AI-assisted technologies in the writing process

During the preparation of this work the authors used ChatGPT and Gemini in order to improve the readability and language of the manuscript. After using these tools, the authors reviewed and edited the content as needed and take full responsibility for the content of the published article.

Declaration of competing interest

The authors declare that they have no known competing financial interests or personal relationships that could have appeared to influence the work reported in this paper.

Acknowledgments

This work has been financed by the Research Fund for the Italian Electrical System under the Three-Year Research Plan 2025–2027 (MASE, Decree n.388 of November 6th, 2024), in compliance with the Decree of April 12th, 2024.

Data availability

The authors are unable or have chosen not to specify which data has been used.

References

[1] O. Kanz, B. Lim, Vehicle-integrated photovoltaics (VIPV) as a core source for electricity in road transport, VIPV position paper – European technology & innovation platform ETIP. https://etip-pv.eu/publications/etip-pv-publications/download/vehicle-integrated-photovoltaics-vipv-as-a-core-so, 2020.

[2] C. Schuss, T. Kotikumpu, B. Eichberger, T. Rahkonen, Impact of dynamic environmental conditions on the output behaviour of photovoltaics, in: Proceedings of the 20th IMEKO TC-4 International Symposium, 2014, pp. 993–998. Benevento, Italy, 15–17 September, https://www.imeko.org/publications/tc4-2014/IMEKO-TC4-2014-437.pdf.

[3] L. San Josè, R. Moruno, R. Núñez, R. Herrero, J. Macías, I. Antón, Performance evaluation of MPPT algorithm of VIPV systems in realistic urban routes using image processing, Sol. Energy Mater. Sol. Cell. 276 (2024) 113061, https://doi.org/10.1016/j.solmat.2024.113061.

[4] M. Jankovec, K. Brecl, M. Bokalic, M. Pir, M. Topic, Monitoring solar irradiance and PV module performance in Mobile applications, Sol. Energy Mater. Sol. Cell. 277 (2024) 113101, https://doi.org/10.1016/j.solmat.2024.113101.

[5] M.Y. Worku, M.A. Hassan, L.S. Maraaba, Md Shafiullah, M.R. Elkadeem, Md I. Hossain, M.A. Abido, A comprehensive review of recent maximum power point tracking techniques for photovoltaic systems under partial shading, MDPI Sustainability 15 (2023) 11132, https://doi.org/10.3390/su151411132.

[6] C. Schuss, T. Fabritius, Impact of environmental conditions on the degree of efficiency and operating range of PV-Powered electric vehicles, Appl. Sci. 12 (3) (2022) 1232, https://doi.org/10.3390/app12031232.

[7] G. Wetzel, L. Salomon, J. Krugener, R. Peibst, Specifications for maximum power point tracking in vehicle-integrated photovoltaics based on high-resolution transient irradiance measurements, Conf. Rec. IEEE Photovolt. Spec. Conf. (2020) 1124–1126, https://doi.org/10.1109/PVSC45281.2020.9300565, 2020-June.

[8] G. Wetzel, L. Salomon, J. Krügener, D. Bredemeier, R. Peibst, High time resolution measurement of solar irradiance onto driving car body for vehicle integrated photovoltaics, Prog. Photovoltaics Res. Appl. 30 (5) (2022) 543–551, https://doi.org/10.1002/pip.3526.

[9] K. Araki, Y. Ota, A. Nagaoka, K. Nishioka, 3D solar irradiance model for nonuniform shading environments using shading (aperture) matrix enhanced by local coordinate system, Energies 16 (2023) 4414, https://doi.org/10.3390/en16114414.

[10] K. Araki, Y. Ota, M. Yamaguchi, Measurement and modeling of 3D solar irradiance for vehicle-integrated photovoltaic, Appl. Sci. 10 (2020) 872, https://doi.org/10.3390/app10030872.

[11] R.M. Chao, S.H. Ko, H.K. Lin, I.K. Wang, Evaluation of a distributed photovoltaic system in grid-connected and standalone applications by different MPPT algorithms, Energies 11 (6) (2018) 121693718, https://doi.org/10.3390/en11061484.

[12] H. Samadi, G. Ala, V. Lo Brano, P. Romano, F. Viola, Investigation of effective factors on vehicles integrated photovoltaic (VIPV) performance: a review, World Electr. Veh. J. 14 (6) (2023) 154, https://doi.org/10.3390/wevj14060154.
[13] M.S. Endiz, G. Gökkus, A.E. Cosgun, H. Demir, A review of traditional and advanced MPPT approaches for PV systems under uniformly insolation and partially shaded conditions, Appl. Sci. 15 (2025) 1031, https://doi.org/10.3390/app15031031.
[14] M. Srikanth, K. Yadlapati, MPPT techniques exploration under uniform and non-uniform solar irradiance Condition–A survey, E3S Web of Conferences 472 (2024) 01024, https://doi.org/10.1051/e3sconf/202447201024.
[15] M.K. Senapati, C. Pradhan, S. Padmanaban, O.A. Zaabi, Photovoltaic MPPT performance adaptability to partial shading resilience and load variations with modified adaptive jaya optimization, IEEE Trans. Consum. Electron. 71 (1) (2025) 734–747, https://doi.org/10.1109/TCE.2025.3532660.
[16] M.K. Senapati, C. Pradhan, R.K. Calay, A computational intelligence based maximum power point tracking for photovoltaic power generation system with small-signal analysis, Optim. Control Appl. Methods 44 (2021) 617–636, https://doi.org/10.1002/oca.2798.
[17] I. Nakir, A. Durusu, H. Akca, A. Ajder, R. Ayaz, E. Ugur, M. Tanrioven, A new MPPT algorithm for vehicle integrated solar energy system, J. Energy Resour. Technol. Trans. ASME 138 (2) (2016) 1–9, https://doi.org/10.1115/1.4031943.
[18] S.A. Rizzo, N. Salerno, G. Scelba, A. Sciacca, Enhanced hybrid global MPPT algorithm for PV systems operating under fast-changing partial shading conditions, Int. J. Renew. Energy Resour. 8 (No.1) (March, 2018).
[19] European patent N. EP3249492B1. https://patentimages.storage.googleapis.com/ef/d0/dd/e0a1c9554c60d6/EP3249492B1.pdf.
[20] A. Minuto, Sviluppo Di Modelli Di Simulazione Del Comportamento Termico Ed Elettrico Di Celle E Moduli Fotovoltaici a Concentrazione E Caratterizzazione Sperimentale, RSE, Prot, 2011 12001235. https://www.rse-web.it/rapporti/sviluppo-di-modelli-per-la-simulazione-del-comportamento-elettrico-di-moduli-e-sistemi-a-concentrazione-e-caratterizzazione-sperimentale-314828/.
[21] M. Herman, M. Jankovec, M. Topič, Optimal I-V curve scan time of solar cells and modules in light of irradiance level, Int. J. Photoenergy (2012) 151452, https://doi.org/10.1155/2012/151452, 11.
[22] P. Casado, J.M. Blanes, C. Torres, C. Orts, D. Marroquí, A. Garrigós, Raspberry Pi based photovoltaic I-V curve tracer, HardwareX 11 (2022) e00262, https://doi.org/10.1016/j.ohx.2022.e00262.
[23] J.I. Morales-Aragonés, M. Dávila-Sacoto, L.G. González, V. Alonso-Gómez, S. Gallardo-Saavedra, L.H. Callejo, A review of I–V tracers for photovoltaic modules: topologies and challenges, Electronics 10 (2021) 1283, https://doi.org/10.3390/electronics10111283.
[24] Ebrar Özkalay, Flavio Valoti, Mauro Caccivio, Alessandro Virtuani, Gabi Friesen, Christophe Ballif, The effect of partial shading on the reliability of photovoltaic modules in the built-environment, EPJ Photovoltaics 15 (7) (2024), https://doi.org/10.1051/epjpv/202400.
[25] Markku Järvelä, Kari Lappalainen, Seppo Valkealahti, Characteristics of the Cloud Enhancement Phenomenon and PV Power Plants, vol. 196, 2020, pp. 137–145, https://doi.org/10.1016/j.solener.2019.11.090.
[26] A. Minuto, E. Celi, G. Timò, N. Panozzo, New maximum power point tracking MPPT algorithm based on research of a target voltage range and its implementation in a commercial inverter for photovoltaic systems, 37th EUPVSEC (2020) 939–944, in: https://userarea.eupvsec.org/proceedings/EU-PVSEC-2020/4DO.7.3/.

Glossary

ADC: Analog - Digital Converter
DC: Direct Current
DSI: Display Serial Interface
FIFO: First In First Out
GTI: Global Tilted Irradiance
HJT: Heterojunction
HMI: Human-Machine Interface
IBC: Interdigitated Back Contact
Isc: Short Circuit Current
I2C: Inter Integrated Circuit
I/O: Inputs/Outputs
MPP: Maximum Power Point
MPPT: Maximum Power Point
PCB: Printed Circuit Board
PERC: Passivated Emitter and Rear Cell
PV: Photovoltaic
P&O: Perturb and Observe
RSE: Ricerca Sistema Energetico
SPI: Serial Peripheral Interface
SW: Software
USB: Universal Serial Bus
VIPV: Vehicle Integrated Photovoltaic
Voc: Open Circuit Voltage